JOURNAL OF GEOPHYSICAL RESEARCH, VOL. 105, NO. B6, PAGES 13,195–13,209, JUNE 10, 2000

Postseismic deformation following the 1906 San Francisco earthquake

Shelley J. Kenner and Paul Segall
Department of Geophysics, Stanford University, Stanford, California

Abstract. We have reevaluated triangulation data from northern California following the 1906 San Francisco earthquake, thereby increasing the temporal and spatial resolution of postseismic deformation following that event. We have calculated uniform shear strain rates and average station velocities at Point Arena using data from 1906-1907, 1929-1930, and 1973-1975 and for the Point Reyes-Petaluma arc using data from 1929-1930, 1938-1939, and 1960-1961. With the addition of recent geodetic data we infer an effective relaxation time for long-term, postseismic deformation following the 1906 earthquake of 36 ± 16 years. The Point Arena data are satisfactorily fit with accelerated afterslip at depth along the San Andreas fault plane. For a 10-km-deep, 25-km-wide afterslip zone the average slip rate between 1906 and 1930 is 11.2 cm/yr. Between 1929 and 1975 it is 4.6 cm/yr. Deformation in the Point Reyes-Petaluma arc is clearly asymmetric with respect to the trace of the San Andreas fault, especially between 1929 and 1939. After inverting for the range of acceptable accelerated deep afterslip and horizontal detachment models, a detailed analysis using geologically reasonable geometries revealed that both model types have trouble explaining the spatial variations in the deformation field through time. In particular, accelerated deep afterslip models cannot reproduce the breadth of the observed deformation field to the northeast of the San Andreas fault. As a result, more complex, time-varying deformation mechanisms are required to explain the Point Reyes-Petaluma arc observations.

1. Introduction

A great earthquake instantaneously disturbs the existing stress balance within the crust and upper mantle. Knowledge of how the resultant stress concentrations are relaxed, both temporally and spatially, can provide information about the deformation mechanisms that drive the earthquake cycle, as well as insight into the structure and rheology of the Earth's crust. Despite this, data on postseismic transients after great strike-slip earthquakes are extremely limited. The temporal resolution, duration, and spatial extent of postseismic data sets are most important for elucidating aspects of earthquake processes that occur over different timescales and length scales. In the first days to months after the 1992 M_w = 7.3 Landers, California earthquake, *Wyatt et al.* [1994] and *Shen et al.* [1994] measured transient deformations that were explained by postseismic afterslip on the rupture plane and its downdip extension. Postseismic transients with durations of a few months to years are seen by *Peltzer et al.* [1996, 1998] and *Savage and Svarc* [1997] using synthetic aperture radar and Global Positioning System (GPS) data. Both *Peltzer et al.* [1996] and *Bosl* [1999] suggest that this deformation can be explained by pore pressure reequilibration. *Peltzer et al.* [1998] show that the multiyear record of post-Landers deformation can be explained by a combination of pore pressure reequilibration and afterslip along portions of the coseismic rupture. Data from the 1989 M = 7.1 Loma Prieta, California, earthquake provide another good example [*Savage et al.*, 1994; *Bürgmann et al.*, 1997]. *Bürgmann et al.* [1997] conclude that short-term postseismic velocity variations can be explained by shallow afterslip on the Loma Prieta fault plane and triggered slip on neighboring thrust faults. This is confirmed by *Pollitz et al.* [1998] who find that to this point, only a small portion of the post-Loma Prieta deformation can be attributed to deep asthenospheric sources. Similar results are seen after the 1994 M = 6.7 Northridge, California, event [*Donnellan and Lyzenga*, 1998]. These studies focus on postseismic transients generated by shallow sources that decay rapidly with time after an event.

Geodetic data spanning the first decades after an event are more likely to provide information about long-period relaxation of structures in the lower crust and upper mantle. The problem is that postseismic data of this temporal extent are generally unavailable, particularly in strike-slip regimes such as California, because of the relatively recent advent of sufficiently accurate geodetic measurements. Also, significant postseismic relaxation of the lower crust and asthenosphere may only be triggered by great strike-slip events. Asthenospheric relaxation has been suggested as an explanation for long-duration, ≥ 5 year, transients [*Savage and Svarc*, 1997] after the 1992 Landers event [*Pollitz et. al.*, 2000, *Deng et al.*, 1998]. Data after the largest events on the San Andreas fault system are limited to triangulation measurements following the 1906 M = 8.3 San Francisco [e.g., *Thatcher*, 1975a, b] and 1857 M = 8 Fort Tejon earthquakes [*Pollitz and Sacks*, 1992].

To date, only uniform shear strain rate estimates are available following the 1906 event (Figure 1). *Thatcher* [1975b], *Cline et al.* [1985], and *Gilbert et al.* [1993] used available geodetic data from the northern California primary arc (Figure 1) to calculate uniform strain rates for various geographic regions, but each region encompasses hundreds of

Paper number 2000JB900076
0148-0227/00/2000JB900076$09.00

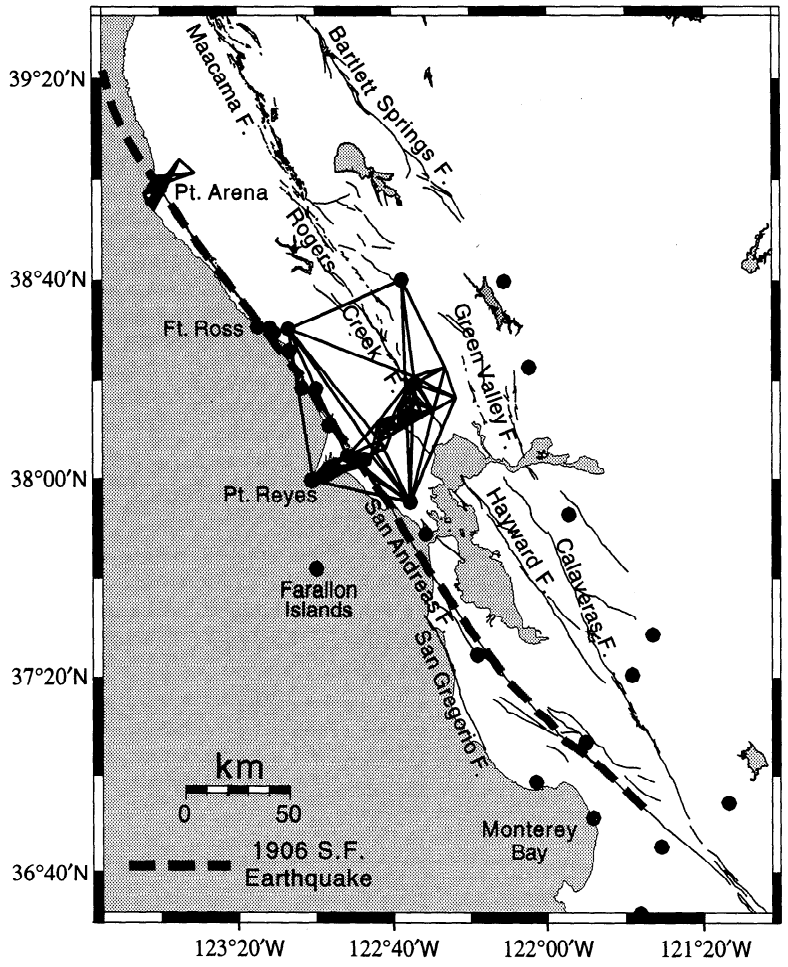

Figure 1. General map showing the location of the Point Arena and Point Reyes-Petaluma networks. The trace of the 1906 San Francisco earthquake is shown by the dashed line. Dark circles denote stations which were used in the northern California primary network inversions.

square kilometers and the uniform strain assumption may not be valid. *Thatcher* [1975a, b] calculated uniform shear strain rates for a number of small aperture networks in northern California, but used only repeated angle measurements. At Point Arena, *Thatcher* [1975a], *Thatcher et al.* [1997], and *Matthews and Segall* [1993] used triangulation data from 1891 to 1906-1907 to estimate the magnitude and depth of coseismic slip during the 1906 earthquake. *Thatcher's* [1975a] results give 5.0 ± 0.05 m of slip to 10 km depth. *Matthews and Segall* [1993] allow for variable slip at depth and estimate a 15-20 km depth of faulting with ~6 m of slip at the surface.

Postseismic studies have computed only total deformation rates following the 1906 San Francisco earthquake. *Thatcher* [1975a] finds that triangulation data between 1906 and 1930 at Point Arena can be satisfactorily explained by ~3.1 ± 0.5 m of slip between 10 and 30 km depth, a slip rate of ~0.13 m/yr. *Thatcher* [1975b] and *Cline et al.* [1985] investigated the post-1906 distribution of shear strain within the Point Reyes-Petaluma arc. Both studies show a nonuniform distribution of deformation with accelerated strain rates at the trace of the Rogers Creek fault. In both cases, anomalous strain rates seen southwest of the San Andreas fault were largely attributed to observational errors. Regardless, both *Thatcher* [1975b] and *Cline et al.* [1985] see decreasing deformation rates when comparing the 1930-1938 and 1938-1961 observation intervals. Finally, *Thatcher* [1983] compiled uniform strain rate estimates from both northern and southern California to infer an ~30 year relaxation time for long-term postseismic deformation within the San Andreas system. The use of strain rates from both northern and southern California could be questioned, however, because, as noted by *Thatcher* [1983], the tectonic regime may be different along the 1906 and 1857 segments of the fault.

In this study, we improve upon prior post-1906 analyses using the methods of *Yu and Segall* [1996], which allow all triangulation measurements, not just repeated angles, to be analyzed. This allows us to include previously unanalyzed triangulation data, especially at Point Arena. With the addition of more recent geodetic data, we are able to determine strain rates at multiple times and infer a relaxation time for long period postseismic deformation along geographically limited segments of the San Andreas fault. We also invert for the distribution of postseismic slip at depth as a function of time. In addition to deep afterslip models we test the applicability of detachment models [e.g., *Furlong et al.*, 1989]. Finally, for each network, we have for the first time been able to estimate station velocities, allowing for a more

detailed investigation of both the spatial and temporal distribution of postseismic deformation after the 1906 earthquake. Information of this type will prove instrumental in discriminating between competing hypothesis regarding deformation mechanisms in northern California [e.g., *Kenner and Segall*, 1999a].

2. Data

Available triangulation data were obtained from the National Geodetic Survey (NGS). The angles between stations were determined from the observed direction lists. For each network or subnetwork, improved station coordinates were then estimated using the triangulation data from all epochs, i.e., ignoring any deformation that might have occurred [*Yu and Segall*, 1996]. If the normalized angle residual to the station adjustment was greater than five standard deviations, it was removed from all stages of the analysis. In general, the direction measurements that were eliminated ended up being suspected blunders, as recorded in the NGS datafiles. Subsequently, observations suspected to be blunders by NGS were removed only if the normalized residual exceeded the largest normalized residual that had not been flagged as a suspected blunder. Though it does not change the qualitative inferences of the work, the quantitative results are somewhat dependent on the details of this procedure.

We concentrated our efforts on two networks, the Point Arena net and the Point Reyes-Petaluma arc. Triangulation surveys (Figure 2) in the vicinity of Point Arena were completed in 1906-1907, 1925, 1929-1930, and 1973-1975. Between 1991 and 1995 a substantial portion of the 1906-1907 network was reoccupied using GPS [*Freymueller et al.*, 1999]. Since stations surveyed in 1925 lie primarily to the northeast of the San Andreas fault and stations surveyed in 1929-1930 lie primarily to the southwest, we chose to analyze the 1906-1907, 1925, and 1929-1930 data sets simultaneously. Though this approach neglects differences in

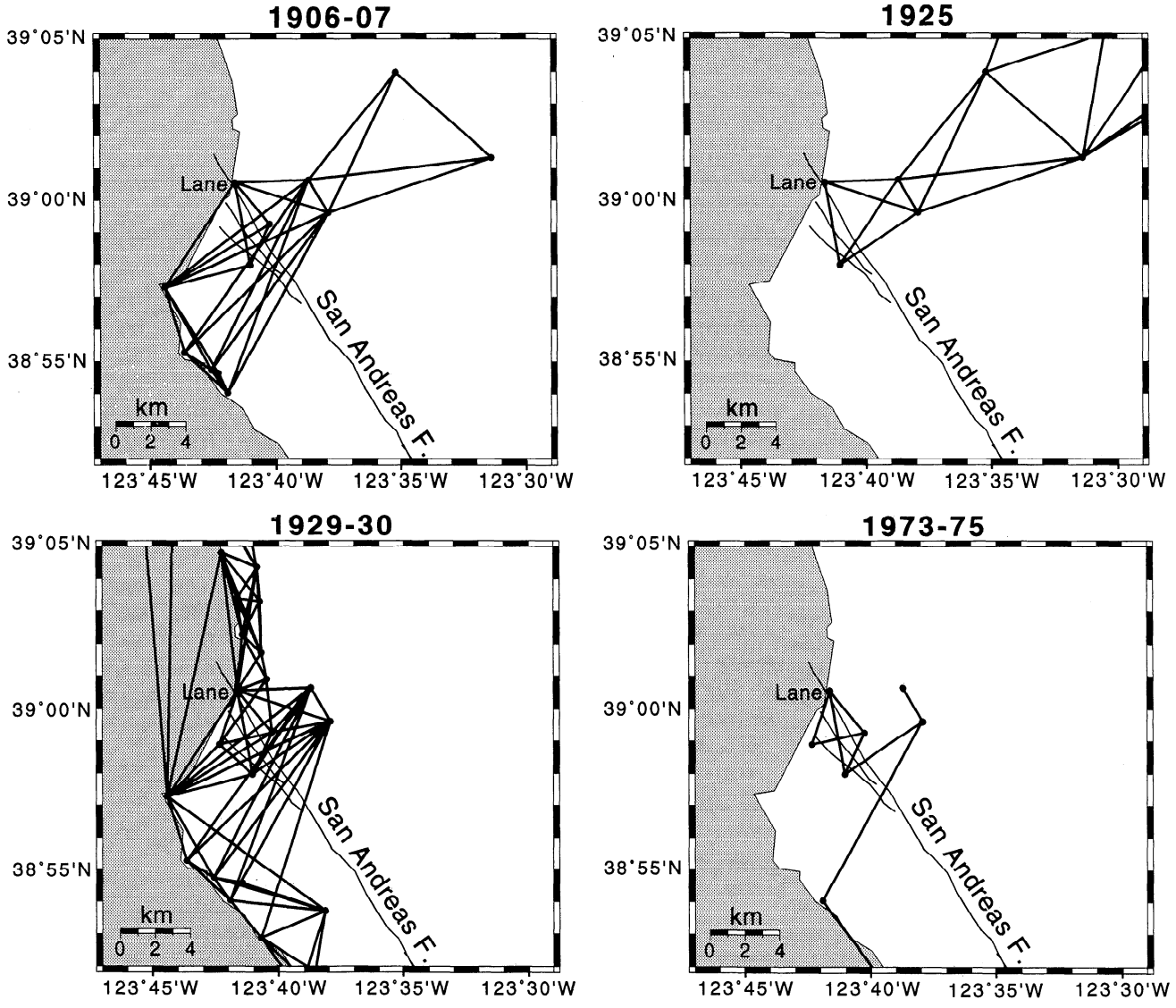

Figure 2. Point Arena surveys of 1906-1907, 1925, 1929-1930, and 1973-1975. The majority of the 1906-1907 network was resurveyed using GPS between 1991 and 1995.

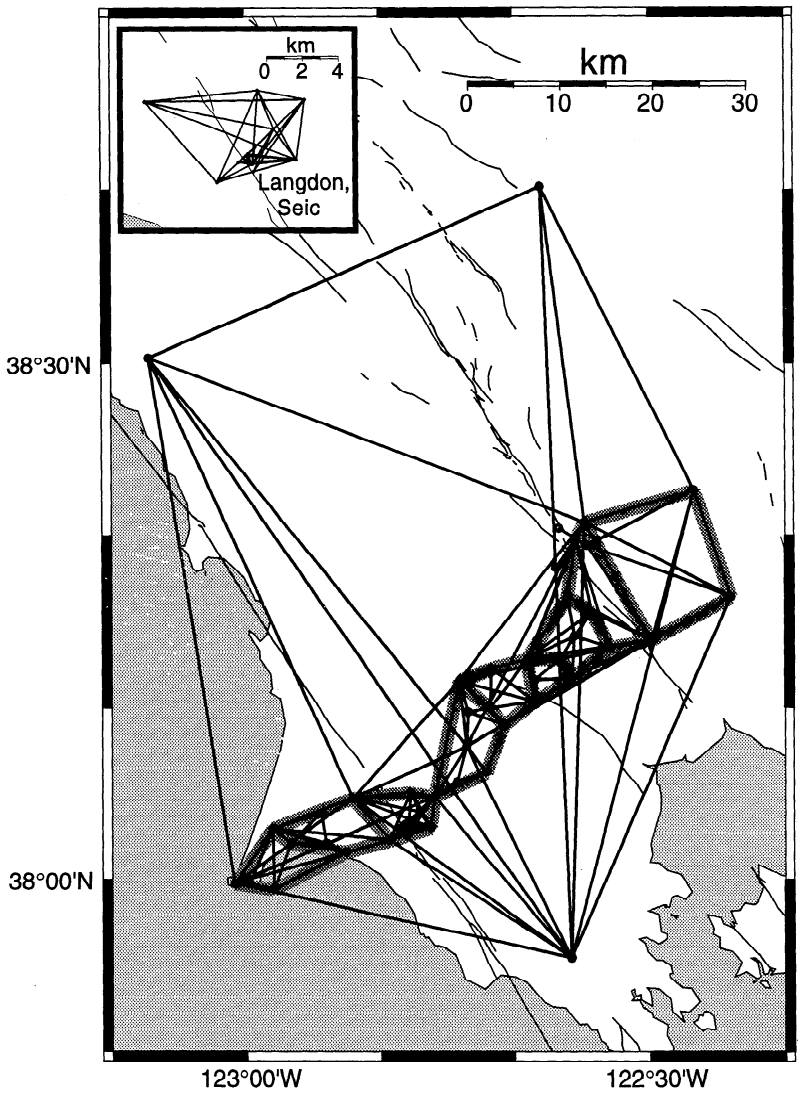

Figure 3. Point Reyes-Petaluma arc surveyed in 1929-1930, 1938-1939, and 1960-1961. Light shaded polygons enclose the subnetworks used to investigate the spatial distribution of uniform shear strain rate within the network. Inset shows the Point Reyes subnetwork. This subnetwork was also surveyed using modern geodetic methods between 1973 and 1991.

the deformation rate during the two time intervals, we feel that the improved spatial resolution compensates for the very minor improvements in temporal resolution that are obtained by analyzing the 1906-1907 to 1925 and 1925 to 1929-1930 data separately. Next, we analyzed the 1929-1930 and 1973-1975 data sets. Given limited network overlap and large uncertainties, a comparison of 1925 and 1973-1975 triangulation data was not warranted. GPS velocities between 1991 and 1995 were taken, without modification, from *Freymueller et al.* [1999]. Though the GPS survey extended much farther to the northeast, we use only those stations that lie within the aperture of the 1906-1907 triangulation network for our calculations.

The Point Reyes-Petaluma arc (Figure 3) extends from Point Reyes Head, ~20 km to the southwest of the San Andreas fault, to the vicinity of Petaluma, ~45 km to the northeast. This entire profile was surveyed in 1929-1930, 1938-1939, and 1960-1961. Subsequent surveys of the region were completed in the 1970s, 1980s, and 1990s using trilateration and/or GPS [*Prescott and Yu*, 1986; *Lisowski et al.*, 1991; *Lisowski and Savage*, 1992; *Williams et al.*, 1994; *Williams*, 1995; *Murray et al.*, 1998; *Savage et al.*, 1999]. We use the results of *Lisowski and Savage* [1992] to complement the historical triangulation data at this location. GPS velocities between 1993 and 1998 [*Murray et al.*, 1998; *Savage et al.*, 1999] are nearly indistinguishable from those of *Lisowski and Savage* [1992], but the station density near the San Andreas fault does not allow for the calculation of shear strain rates in small fault-crossing networks, as required for direct comparison with the triangulation data.

Parts of the northern California primary network were surveyed in 1906-1907, 1922-1923, 1925, 1929-1930, and 1948 (Figure 1). The total aperture of the network is > 120 km. It includes the Farallon Islands, located ~40 km southwest of the San Andreas fault. Estimates of station velocities in a network of this spatial and temporal extent would allow greater resolution of the distribution of post-1906 deformation, particularly to the southwest of the San

Andreas fault. Unfortunately, though we were able to reproduce the uniform strain values of *Thatcher* [1975a], reasonable velocity estimates for the primary network were not obtained. While typical baselines in the Point Reyes-Petaluma and Point Arena networks average under 10 km, baselines in the primary network are tens of kilometers in length with some extending to 90 km. As a result, the uncertainties in the velocity determinations are unacceptably large. Additionally, many of the baselines run along the coastline and may be subjected to large refraction errors resulting from unmodeled gradients in the index of refraction [see *Bomford*, 1980, Sections 1.36-1.37].

3. Analysis

3.1 Uniform Shear Strain Rates

Uniform shear strain rates were calculated from the triangulation data using the approach of *Yu and Segall* [1996]. Uniform shear strain rates associated with the modern geodetic data were calculated from the published station velocities. The best fitting exponential decay rate for the fault parallel shear strain rate was then determined using a least squares solution to a linear reparameterization of the strain rate data in semilog space. This provides an estimate of the average effective exponential relaxation time for time-dependent deformation in the crust and upper mantle following the 1906 San Francisco earthquake. The relaxation time is defined as twice the effective viscosity divided by the shear modulus. The approach presumes that the data in the original parameterization are non-Gaussian [*Menke*, 1989, p. 147]. Though this is not necessarily the case, given the limited number of data, we felt that a more complicated approach was not warranted. In addition, inversions for the best fitting model in semilog space account for the fact that the strain rates represent averages over multiyear time intervals. Since the inversion is linear in this case, the average ln(strain rate) during any time interval is equivalent to the ln(strain rate) at the median or representative time of that interval. An exponential fit is used because this is the form of the first term in the analytical series solution for surface strain rate in an elastic plate overlying a viscoelastic half-space [*Nur and Mavko*, 1974; *Savage and Prescott*, 1978]. It has been shown that a model of this type can satisfactorily approximate the postseismic response of the San Andreas fault system after great events [*Thatcher*, 1983].

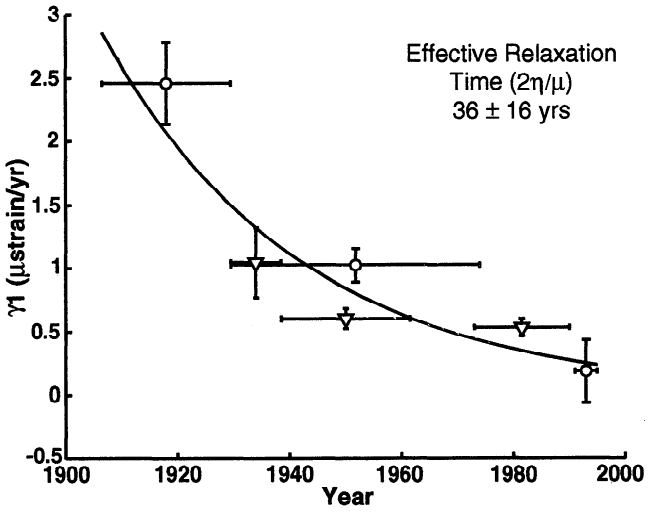

Figure 4. Evolution of uniform shear strain rate with time since the 1906 San Francisco earthquake at Point Arena (circles) and Point Reyes (triangles). Vertical error bars give 1σ uncertainties. Horizontal error bars give the time between the first and last surveys included in the inversion. The solid line is the best fitting exponential regression to the data. Strains have been rotated 20° (clockwise) and 10° (clockwise), respectively, from north so that γ_1 represents the right-lateral shear strain rate across that San Andreas fault.

At Point Arena, uniform shear strain rates between 1906-1930, 1929-1975, and 1991-1995 yield a best fitting exponential relaxation time of 29 ± 15 years. Uniform shear strain rates for a subset of the Point Reyes-Petaluma arc, the Point Reyes network (Figure 3, inset) of *Thatcher* [1975a, 1983], for the time periods 1929-1939, 1938-1961, and 1973-1990 are also determined. Using these shear strain rates, the best fitting exponential relaxation time for postseismic deformation at Point Reyes is estimated to be 79 ± 30 years, but data immediately following the 1906 earthquake, when the rates of change are highest, are unavailable. Combining the Point Arena and Point Reyes data yields a 36 ± 16 year estimate of the relaxation time in northern California (Figure 4). If the average shear modulus of the relaxing materials is assumed to be 6×10^4 MPa [*Thatcher*, 1983], this corresponds to an effective viscosity of $\sim 3.4 \times 10^{19}$ Pa·s.

Additional subnetworks of the Point Reyes-Petaluma arc (Figure 3) were used to investigate the spatial distribution of shear strain for the time periods 1929-1939 and 1938-1961 using the *Yu and Segall* [1996] methodology (Figure 5). During the 1929-1939 time interval, relatively high maximum shear strain rates are broadly distributed between the San Andreas and Rogers Creek faults. Shear strain rates between 1938 and 1961 are generally smaller than those between 1929 and 1939. The only exception are the two subnetworks that include the Rogers Creek fault and areas to the northeast. In both time periods the shear strain rate profile is asymmetric with respect to the trace of the San Andreas fault. Estimated directions of maximum right-lateral shear are more consistent with the strike of the San Andreas fault during the second time interval than during the first.

These same networks and subnetworks were used by *Thatcher* [1975a, b] and *Cline et al.* [1985]. Though the solutions are based on the same data, in some instances they differ at the 1σ level. At Point Arena our results agree with those of *Thatcher* [1975a, 1983]. For the Point Reyes-Petaluma arc our solution has fewer outliers and seems to vary more smoothly with distance from the San Andreas fault than the results of *Thatcher* [1975b] and *Cline et al.* [1985]. This may reflect use of a more robust method for dealing with historical triangulation data. We include more angle measurements than *Thatcher* [1975b], while *Cline et al.* [1985] calculate strains from least squares determined displacements. *Cline et al.* [1985] also include long baselines extending to Fort Ross and Mount Tamalpais. While inclusion of these baselines is beneficial when estimating displacements in long narrow networks, such as the entire Point Reyes-Petaluma arc, inversions for strain using small networks yields higher spatial resolution. As a consequence, we prefer to calculate uniform shear strain rates directly from the data using only those stations within each subnetwork.

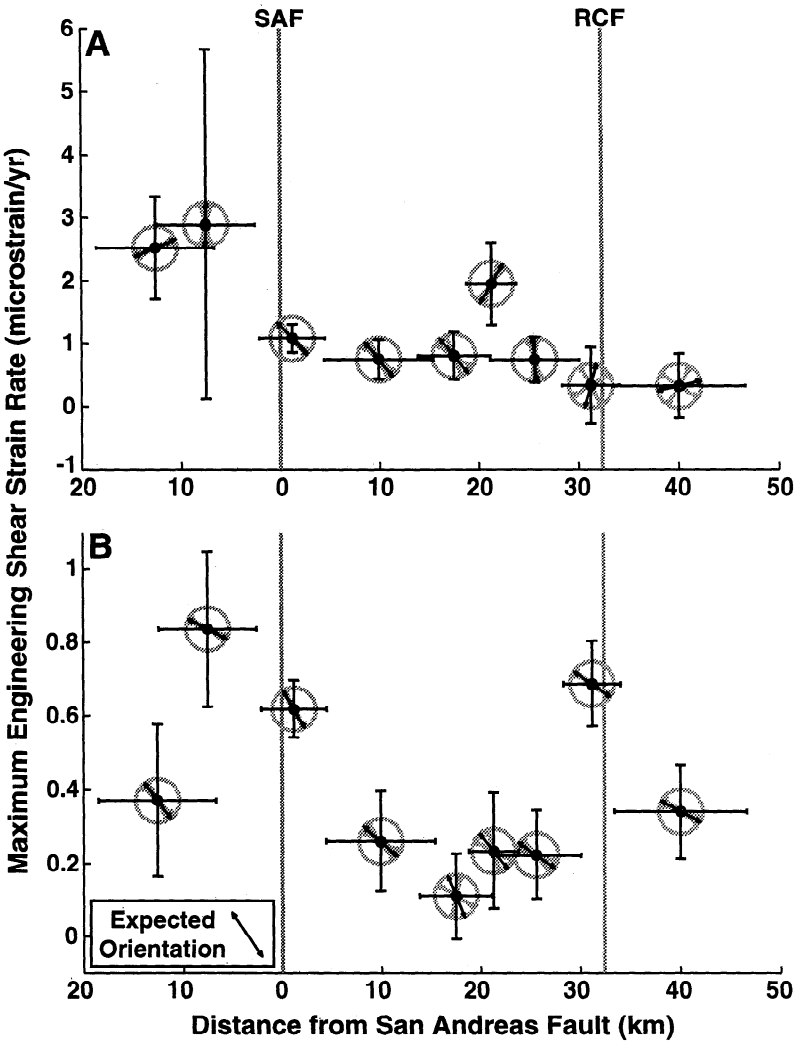

Figure 5. Maximum horizontal engineering shear strain rate (μstrain/yr) and orientation of the maximum right-lateral shear strain rate within the Point Reyes-Petaluma arc between (a) 1929 and 1939 and (b) 1938 and 1961. Vertical error bars give 1σ uncertainty in the magnitude. Horizontal error bars give the lateral extent, in the fault parallel direction, of the subnetwork in which the calculation was made. The dark arrow gives the direction of maximum right-lateral shear. A vertical arrow indicates shear across a plane which strikes in a north-south direction. Lighter arrows define the 1σ uncertainty in the direction of maximum right-lateral shear. At the location of the Point Reyes-Petaluma arc the San Andreas fault is at an orientation of ~N35°W. Note the different scales in Figures 5a and 5b.

The variations among the different solutions may also reflect differences in how suspected blunders were treated.

3.2 Inversions for Slip at Depth

Assuming post-1906 deformation can be adequately represented by afterslip at depth, we attempt to infer the distribution of slip as a function of time on either the downdip extension of the 1906 rupture or a detachment lying northeast of the San Andreas fault. Specifically, for each time interval being considered, we use an elastic dislocation model to invert for acceptable distributions of slip at depth. Unfortunately, the triangulation networks are not broadly distributed about the San Andreas fault, severely limiting depth resolution. The limited resolution forced us to divide the San Andreas fault into only three depth intervals. The shallowest interval represents the seismogenic fault, which is assumed to be locked following the earthquake. The second depth interval represents a zone of accelerated postseismic afterslip. The third interval extends to infinite depth and represents deep slip at a constant rate of 20 mm/yr [*Kelson et al.*, 1992; *Freymueller et al.*, 1999]. Free parameters in the accelerated afterslip model are the depth to the top and width of the afterslip zone and the rate of fault slip. Detachment model parameters are depth, fault-perpendicular width of the detachment surface, and slip rate. The southwestern edge of the detachment surface is assumed to be colocated with the trace of the San Andreas fault. To test the hypothesis that the deep plate boundary is located northeast of the San Andreas fault, no slip is allowed below the detachment surface along the San Andreas fault. Also, the Hayward-Rogers Creek-Maacama fault is assumed to slip at 30 mm/yr below the level of the detachment surface. This is approximately equal to the combined San Andreas and Hayward-Rogers Creek-Maacama fault slip rates [*Bürgmann et al.*, 1994, 1997]. Shallow creep,

in accordance with the secular model, is also allowed. As models incorporating a viscoelastic lower crustal channel or asthenosphere [*Thatcher*, 1983; *Li and Rice*, 1987; *Savage*, 1990] would likely be indistinguishable from the deep afterslip model on the basis of this dataset [*Savage*, 1990], they are not explicitly addressed.

In each inversion, the secular model of *Bürgmann et al.* [1994, 1997] is used to model slip on all faults other than the portion of the San Andreas and/or Hayward-Rogers Creek-Maacama faults being considered. The secular model extends from approximately the latitude of Parkfield, California, north to Point Arena. For our purposes the three subparallel faults in northern California were extended from Point Arena to Cape Mendocino. They were modeled as single fault segments slipping below ~10 km depth.

The slip model minimizing the weighted residual sum of squares was found using a simple grid search. A linear least squares solution was used to specify the optimal slip rate for each set of geometric parameters (depth and width). Confidence intervals were derived using an F test [e.g., *Árnadóttir and Segall*, 1994]. In spite of the fact that this approach underestimates actual confidence limits [*Árnadóttir and Segall*, 1994], our results indicate the data place only weak constraints on the depth extent of afterslip. This is not surprising given the spatial extent of the networks. Additional constraints can be applied if we assume that the 1906 San Francisco earthquake was a characteristic event and neglect plastic deformation in the crust adjacent to the fault (i.e., we assume that at long timescales the lithospheric plates move as rigid bodies). Using these assumptions, we can state that

$$\int_{T_{\text{cycle}}} \dot{s}(t)dt = S, \tag{1}$$

where $\dot{s}$ is the slip rate at any depth, S is the characteristic earthquake slip, and T_{cycle} is the characteristic earthquake cycle time. If (1) is discretized into finite temporal epochs, we have

$$\sum_{i=1}^{n} \dot{\bar{s}}_i (t_{i+1} - t_i) \cong S, \tag{2}$$

where $\dot{\bar{s}}$ is the average slip rate during time interval (t_{i+1} - t_i). Using (2), we can then bound the slip rate during any particular time interval by assuming that S provides an upper bound on the amount of slip that can take place in any depth interval during one complete earthquake cycle:

$$\dot{\bar{s}}_i \le \frac{S}{(t_{i+1} - t_i)}. \tag{3}$$

If we have estimates of the slip during one or more prior intervals, then at any depth we can use (2) to generate more detailed constraints of the form

$$\dot{\bar{s}}_i \le \frac{S - \sum_{\substack{\text{Prior} \\ \text{Estimates}}} \dot{\bar{s}}_j (t_{j+1} - t_j)}{(t_{i+1} - t_i)}. \tag{4}$$

Given the limited depth resolution of the data, we assume that the depth extent of the accelerated afterslip zone does not change with time. Especially at Point Arena, we find slip rate constraints of this type, based on the expected characteristic slip, to be more restrictive than the formal confidence intervals. Estimates of the amount of coseismic slip during the 1906 San Francisco earthquake range from ~5 to 7 m [*Thatcher*, 1975a; *Thatcher et al.*, 1997, *Matthews and Segall*, 1993]. All results are summarized in Table 1. Because uncertainties in the model inversions are large, only model bounds, as defined by the slip rate constraint and the 95% confidence interval, are listed.

Optimal slip rates for a deep afterslip model of deformation between 1906-1930 and 1929-1975 at Point Arena are shown in Plates 1a and 1b. For both time intervals the data constrain the top of the zone of postseismic slip to be no shallower than 1-2 km. Owing to the narrow aperture of the network, the width of the zone of accelerated afterslip is unconstrained. Between 1906 and 1930 the 95% confidence level and a slip rate constraint (equation (3)) requires that the top of the postseismic afterslip zone be no deeper than 20 km. Allowable slip rates are between ~2 and 24 cm/yr. During the 1929-1975 time interval a slip rate constraint that includes prior slip between 1906 and 1930 (equation (4)) requires the top of the postseismic afterslip zone be no deeper that 12.5 km. For each set of geometric parameters the appropriate 1906-1930 slip rate is used in the constraint calculation. Allowable 1929-1975 slip rates are between ~0 and 5.8 cm/yr. If the accelerated afterslip zone is constrained to be 25 km wide with a top depth of 10 km, consistent with 1) the slip rate constraint during both time intervals, 2) the maximum depth of seismicity in California, and 3) *Thatcher's* [1975a] estimate of the depth of coseismic faulting during the 1906 earthquake, the slip rate evolves with time as shown in Figure 6.

Inversion results for the best fitting accelerated afterslip zone during the 1929-1939 time interval at Point Reyes-Petaluma are shown in Plate 1c. At 95% confidence the top of the afterslip zone must be above 21.5 km depth, while the width is entirely unconstrained. Slip rates range between ~0 and 53 cm/yr. The slip rate constraint (equation (3)) is less

Table 1. Inversion Results

	Deep Accelerated Afterslip Model			Detachment Model		
Network	Top Depth, km	Width of Afterslip Zone, km	Slip Rate, cm/yr	Top Depth, km	Width, km	Slip Rate, cm/yr
Point Arena network						
1906-1930	1-20	2*	2.0-24.0	-	-	-
1929-1975	0-13	2*	0.0-5.8	-	-	-
Point Reyes-Petaluma arc						
1929-1939	0-22	2*	0.0-53.0	3-36	29-54	1.5-10.0
1938-1961	0-20	2*	0.0-18.0	5-13	29-38	1.0-3.0

Acceptable model minimum and maximum bounds are based on the slip rate constraint and 95% confidence level.

* Width is required to be at least 2 km in the inversion. Maximum widths are not well constrained by the inversion for most parameter combinations.

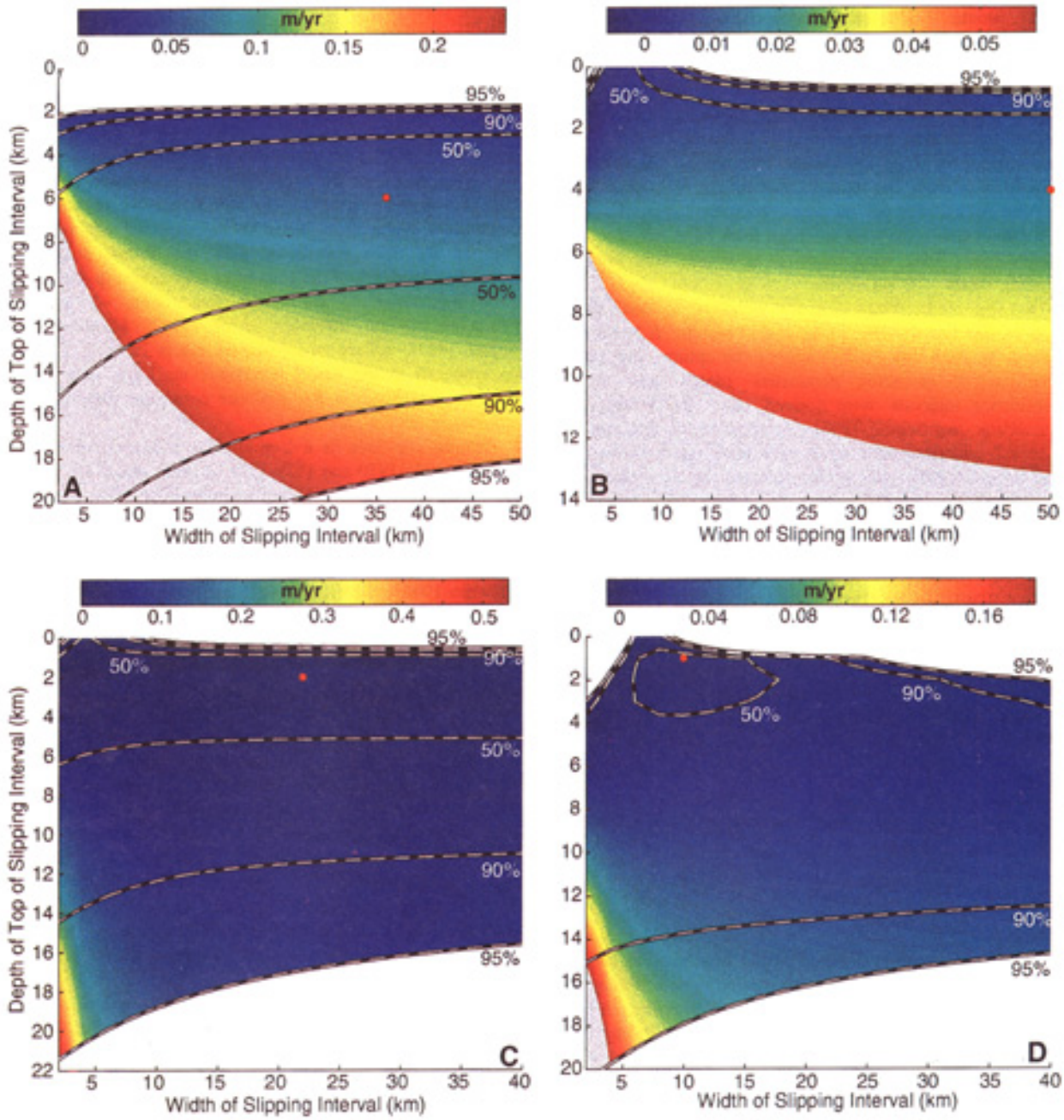

Plate 1. Optimal slip rate as a function of the top depth and width of the zone of accelerated afterslip for the deep afterslip model at the Point Arena network between (a) 1906 and 1930 and (b) 1929 and 1975 and for the Point Reyes-Petaluma arc between (c) 1929 and 1939 and (d) 1938 and 1961. Optimal models, shown by the red asterisk, give Plate 1a) a slip rate of 62 mm/yr between 6 and 42 km (misfit of 1.053), Plate 1b) a slip rate of 16 mm/yr between 4 and 54 km (misfit of 1.035), Plate 1c) a slip rate of 10 mm/yr between 2 and 24 km (misfit of 1.389), and Plate 1d) a slip rate of 2 mm/yr between 1 and 11 km (misfit of 1.243). Black lines with white dashes denote 50%, 90%, and 95% confidence levels. White areas are not allowed at 95% confidence. Gray areas are excluded using the characteristic slip constraint that allows 5.5 m of coseismic slip at Point Arena and 6.5 m at the Point Reyes-Petaluma arc. In Plates 1a and 1c the slip constraint is derived using equation (3). In Plates 1b and 1d the slip constraint is derived using equation (4) and slip rates from the 1906-1930 Point Arena inversion and 1929-1939 Point Reyes-Petaluma inversion, respectively.

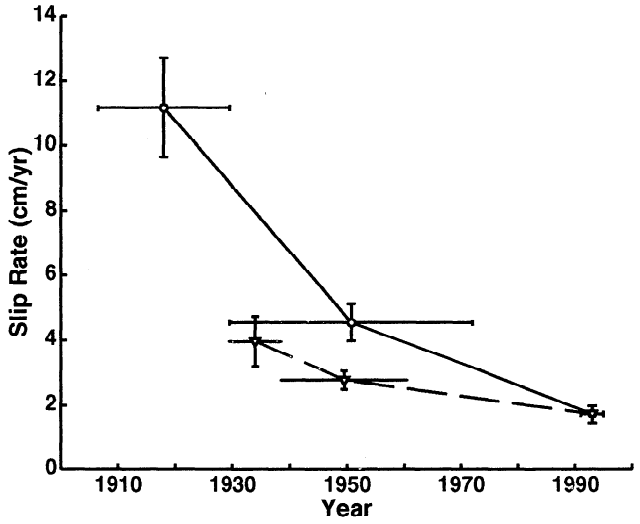

Figure 6. Slip rate as a function of time since the 1906 San Francisco earthquake at Point Arena (circles) and the Point Reyes-Petaluma arc (triangles) for a 25-km-wide, deep accelerated afterslip zone whose top is located at 10 km depth. The slip rate between 1991 and 1995 is taken from the results of *Freymueller et al.* [1999] for all of northern California. Vertical error bars give 1σ uncertainties. Horizontal error bars give the time between the first and last surveys included in the inversion.

restrictive than the 95% confidence level in this case. The data from the 1938-1961 interval can be fit with a deep afterslip model that has between 0 and 18 cm/yr of slip with the top of the accelerated afterslip zone located above 19.5 km (Plate 1d). Both the slip rate constraint (equation (4)) and triangulation data constrain this result. The optimal deep afterslip model requires 2 mm/yr of slip between 1 and 11 km, essentially the range of coseismic faulting. Below this depth the fault slips at the secular rate, 20 mm/yr. This optimal model is consistent with a fault that is essentially locked at seismogenic depths. Both Point Reyes-Petaluma inversions have a normalized misfit that is 1.2-1.3 times higher than the Point Arena results. For a 25-km-wide afterslip zone located below 10 km depth, the slip rate, at any given time, is generally smaller than the slip rate at Point Arena (Figure 6). In both case, slip rates along the downdip extension of the San Andreas fault decrease monotonically with time since the 1906 San Francisco earthquake.

Detachment models fit the 1929-1939 Point Reyes-Petaluma data as well as deep afterslip models do. At 95% confidence a detachment surface extending northeast of the San Andreas fault can be between 3 and 36 km deep and between 29 and 64 km wide. Allowable slip rates are between ~1.5 and 10 cm/yr. The optimal model (misfit of 1.390) gives 2.5 cm/yr of slip on a 6-km-deep, 34-km-wide detachment surface. The 1938-1961 data can be optimally fit (misfit of 1.248) with 2.1 cm/yr of slip on an 8-km-deep, 32-km-wide detachment surface. At 95% confidence the detachment surface can be between 5.5 and 13 km deep and between 29 and 38 km wide. Allowable slip rates are between ~1.0 and 3.0 cm/yr. During both time periods the optimal detachment surface is too shallow to satisfy independent evidence based on the maximum depth of seismicity in northern California, the depth of coseismic faulting in 1906 [*Thatcher*, 1975a; *Matthews and Segall*, 1993], and the seismic reflection data [*Holbrook et al.*, 1996].

3.3 Station Velocity Estimates

Velocity estimates were obtained from the triangulation data using a slightly altered form of the methods described by *Yu and Segall* [1996]. They solved for the station displacements using data from two different triangulation surveys. We generalized their method, solving for station velocities using data from an arbitrary number of surveys. As described by *Yu and Segall* [1996], the initial station coordinates $\mathbf{x}_1$ are obtained using an iterated minimum norm solution to update the a priori station coordinates. Using the notation of *Yu and Segall* [1996], the observation equations, linearized about these coordinates [*Yu and Segall*, 1996, equations (6) and (7)], are

$$\mathbf{d}\theta_n = A_n \mathbf{dx}_n + \varepsilon_n \qquad n = 1, 2, \ldots m, \tag{5}$$

where m is the number of different surveys that will be included in the inversion, A_n represents the network geometry at time t_n with stations at coordinates $\mathbf{x}_n$, ε_n are the measurement errors, and $\mathbf{d}\theta_n = \theta_n(\mathbf{x}) - \theta_n(\mathbf{x}_1)$ represents the difference between the observed angles and those estimated from the initial station coordinates, $\mathbf{x}_1$, at time t_1, the time of the earliest survey. The change in position for all subsequent surveys can then be defined as

$$\mathbf{dx}_n = \mathbf{dx}_1 + \mathbf{v}dt_n, \tag{6}$$

where $\mathbf{v}$ are the station velocities, $dt_n = t_n - t_1$, and t_n is the date of survey n. If a survey took place over multiple years, it was assigned a date representative of the midpoint of its duration; for example, the 1929-1930 survey was assigned a date of 1929.5. The full system of equations can now be written as

$$\begin{bmatrix} \mathbf{d}\theta_1 \\ \mathbf{d}\theta_2 \\ \vdots \\ \mathbf{d}\theta_n \end{bmatrix} = \begin{bmatrix} A_1 \\ A_2 \\ \vdots \\ A_n \end{bmatrix} \mathbf{dx}_1 + \begin{bmatrix} 0 \\ A_2 dt_2 \\ \vdots \\ A_n dt_n \end{bmatrix} \mathbf{v} + \begin{bmatrix} \varepsilon_1 \\ \varepsilon_2 \\ \vdots \\ \varepsilon_n \end{bmatrix}, \tag{7}$$

which for compactness can be rewritten as

$$\mathbf{d}\theta = \Psi \mathbf{dx} + \Omega \mathbf{v} + \varepsilon, \quad \varepsilon \sim N(0, \Sigma), \tag{8}$$

where

$$\Sigma = \begin{pmatrix} \Sigma_1 & 0 & 0 & 0 \\ 0 & \Sigma_2 & 0 & 0 \\ 0 & 0 & \ddots & 0 \\ 0 & 0 & 0 & \Sigma_n \end{pmatrix} \tag{9}$$

and Σ_i are the data covariances for each survey. Equations (8) and (9) are equivalent to equations (10) and (11) of *Yu and Segall* [1996]. The station velocities are then determined using exactly the same procedure that *Yu and Segall* [1996] used for determining station displacements, except that $\mathbf{u}$ is replaced by $\mathbf{v}$ in all subsequent equations. As before, corrections to the station coordinates are removed from the governing equations by premultiplying (8) by $(I - \Psi\Psi^{\dagger})$ where $\Psi^{\dagger}$ is the generalized inverse of Ψ. Since triangulation data do not constrain rigid body rotations, translations, or dilatation, we present model coordinate velocities [*Segall and*

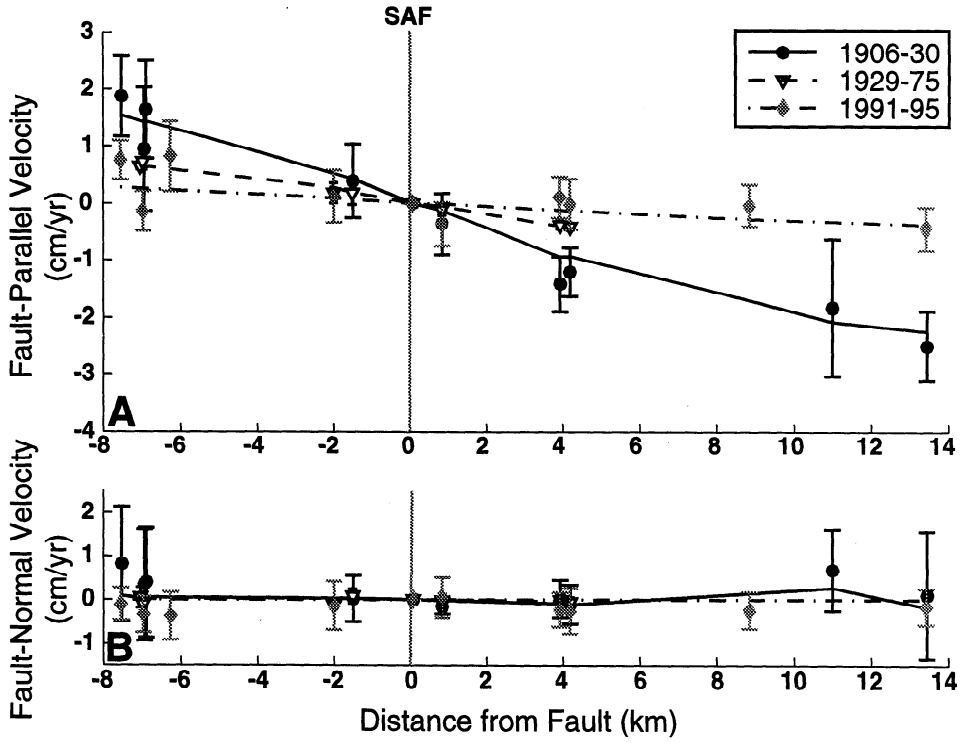

Figure 7. Total (a) fault-parallel (N25°W) and (b) fault-normal model coordinate velocities, with 1σ uncertainties, as a function of distance from the San Andreas fault at Point Arena. Model coordinate velocities are estimated using a 25-km-wide afterslip zone whose top is located at 10 km depth. The slip rates are 11.2 cm/yr and 4.6 cm/yr for the 1906-1930 and 1929-1975 periods, respectively (Figure 6). Velocities are plotted relative to the velocity at station Lane. Model predictions are given by the appropriate lines. The model for the 1991-1995 GPS velocities is taken from the inversion results, using data from all of northern California, of *Freymueller et al.* [1999] for the San Andreas fault that give 17.4 mm/yr of slip below 14.9 km depth.

Matthews, 1988]. Solutions of this type depend on a prior model to provide a reference frame for the solution and constrain the null space, those components of the solution that are not constrained by the data. In practice, since network rotations and strike-slip deformation look the same in narrow fault-perpendicular networks, use of model coordinate velocities means that increasing the amount of slip at depth on the San Andreas fault in the prior model increases the resultant velocities in an antisymmetric sense about the San Andreas fault. This effect is most pronounced in the Point Arena network. Because the Point Reyes-Petaluma arc is braced by stations at Mount Tamalpais, Ross Mountain, and Mount Helena, the effect is significantly reduced.

The model coordinate station velocity estimates at Point Arena are derived using the best fitting model with afterslip between 10 and 35 km depth (Figure 7). Secular slip rates are applied to all other faults and depth intervals. As shown, the computed velocities on either side of the fault clearly decrease and become smoother with time. Further, they are consistent with the prior model. While this does not mean that the model is correct, it does mean that it is consistent with the spatial distribution of deformation. When only the secular model of *Bürgmann et al.* [1994, 1997] is used to constrain the null space, the trends in the resultant velocities, which represent a probable minimum bound on fault-parallel velocity magnitudes, are still discernible, though the prior model is clearly inconsistent with the 1906-1930 data.

The Point Reyes-Petaluma arc velocities as determined using the best fitting model with afterslip between 10 and 35 km depth are given in Figure 8. During the 1929-1939 time interval the prior model is inconsistent with the data. It is more appropriate during the 1938-1961 interval, though the fault parallel velocities are still slightly underpredicted. Regardless, it is apparent that velocities to the northeast of the San Andreas fault decrease with time following the 1906 San Francisco earthquake. This variation in velocity with time remains even when a purely secular prior model is used to constrain the null space. The trends in the velocity distribution through time to the southwest of the fault are more problematic. The 1929-1939 velocities show little shear strain accumulation and possess a component of fault normal contraction within ~20 km of the San Andreas fault. Shear strain rates for the same region (Figure 5a) are highly uncertain with directions of maximum right-lateral shear strain which are inconsistent with the regional deformation field. This anomalous deformation was previously attributed to observational errors by *Thatcher* [1975b] and *Cline et al.* [1985]. Geometric inconsistencies in the network at this location probably contribute as well. In spite of this, the 1929-1939 results clearly indicate important postseismic spatial variations and asymmetries in the deformation field at the latitude of Point Reyes.

4. Discussion

As mentioned, the quantitative results are, to a certain extent, a function of how suspected blunders were dealt with during initial processing of the triangulation data. Changes

are only significant for the slip inversions and velocity estimates involving data from the entire Point Reyes-Petaluma arc in 1929-1930. Other networks, subnetworks, and time intervals contain fewer suspected blunders so that the solutions are less sensitive to the treatment of outliers. In the extreme, if all suspected blunders and data of questionable reliability from the southwest of the San Andreas are removed from the 1929-1930 Point Reyes-Petaluma data set, inversions for slip at depth are far less constrained and the inferred slip rates are lower for any given geometry. Estimated model coordinate velocities to the northeast of the San Andreas fault between 1929 and 1939 are also lower, though they are still slightly higher than during the 1938-1961 time interval and the nearly linear trend in velocity northeast of the San Andreas fault persists. Inversions using this reduced data set have a normalized misfit that is ~8% smaller than inversions using the entire data set.

Prior analyses of postseismic deformation following the 1906 San Francisco earthquake have not been very detailed because they have been limited to estimates of uniform shear strain rate and simple dislocation models with assumed a priori constraints. With the improved methods of *Yu and Segall* [1996] and the addition of more recent geodetic results, we have been able to obtain much better spatial and temporal resolution of postseismic deformation following the 1906 earthquake. Estimates of the relaxation time for long-term postseismic deformation at Point Arena and Point Reyes are in agreement with estimates of ~30 years made by *Thatcher* [1983] for the entire San Andreas fault. This supports the conclusion that there are long-term postseismic transients, probably generated by deep sources in the lower crust and upper mantle, after great events within the San Andreas fault system.

The presence of long-term postseismic transients is also discernible in our estimates of the spatial distribution of deformation. We find that geodetically observable deformation transients following the 1906 earthquake have, within observational uncertainties, largely disappeared by about 1940. Shear strain rates within the Point Reyes-Petaluma arc generally decay with time. The primary exception is the subnetwork that crosses the Rogers Creek fault. This may be explained by the fact that the 1906 San Francisco earthquake moved both the shear stress and the Coulomb failure function on the Rogers Creek fault away from failure [*Simpson and Reasenberg*, 1994; *Jaumé and Sykes*, 1996; *Kenner and Segall*, 1999a]. Postseismic strain accumulation and creep rates immediately following the 1906 earthquake would therefore be expected to be lower at this location. Velocities at both the Point Arena and Point Reyes-Petaluma arcs are also higher during the earliest time intervals. During subsequent time intervals the velocities are nearly indistinguishable from the modern geodetic results.

Our deformation estimates provide snapshots of the evolution of the spatial distribution of postseismic

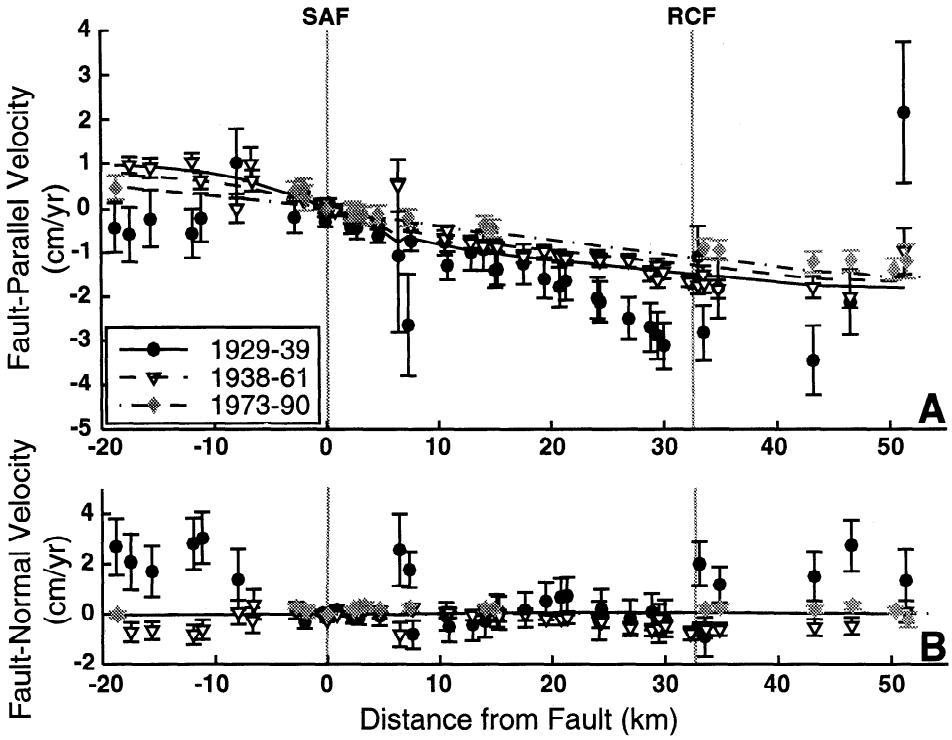

Figure 8. Total (a) fault-parallel (N35°W) and (b) fault-normal model coordinate velocities, with 1σ uncertainties, as a function of distance from the San Andreas fault for the Point Reyes-Petaluma arc. Model coordinate velocities are estimated using a 25-km-wide afterslip zone whose top is located at 10 km depth. The slip rates are 4.0 cm/yr and 2.8 cm/yr for the 1929-1939 and 1938-1961 periods, respectively (Figure 6). Triangulation results are plotted relative to the velocity at Langdon. The 1973-1990 velocities [*Lisowski and Savage*, 1992] are plotted relative to the velocity at a nearby station, Seic. Model predictions are given by the appropriate lines. The 1973-1990 results are plotted with the secular model of *Bürgmann et al.* [1994, 1997].

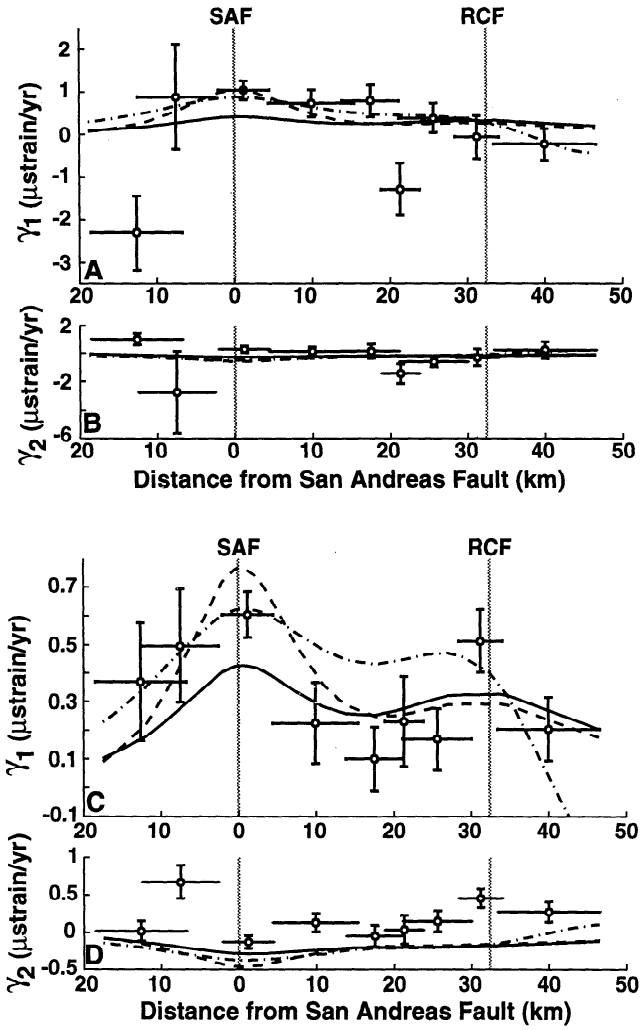

Figure 9. Shear strains within the Point Reyes-Petaluma arc between (a) and (b) 1929 and 1939 and (c) and (d) 1938 and 1961. Model results are shown for a purely secular prior model (solid), a model with postseismic afterslip slip between 25 and 50 km on the San Andreas fault (dashed), and a model that includes a horizontal detachment at 15 km depth that extend 45 km to the northeast of the San Andreas fault (dash-dotted). Slip rates in the accelerated afterslip model are 4.0 and 2.8 cm/yr for the 1929-1939 and 1938-1961 periods, respectively (Figure 6). Slip rates in the detachment model are 4.3 and 3.0 cm/yr for the 1929-1939 and 1938-1961 periods, respectively. Here γ_1 represents the right-lateral shear strain rate across that San Andreas fault (N35°W) and γ_2 represents shearing associated with unilateral extension or compression perpendicular to the trace of the San Andreas fault (tension positive). Vertical error bars give the 1σ uncertainty in the magnitude. Horizontal error bars give the lateral extent, in the fault-parallel direction, of the subnetwork in which the calculation was made.

deformation at Point Arena and Point Reyes through time. Recent geodetic data indicate that the velocity field [*Freymueller et al.*, 1999; *Williams et al.*, 1994; *Lisowski et al.*, 1991; *Prescott and Yu*, 1986] is not antisymmetric about the trace of the San Andreas fault, as one would expect if the San Andreas accommodates the majority of the Pacific-North American relative plate motion. Postseismic velocities from Point Arena do not exhibit profound asymmetries with respect to the trace of the San Andreas fault, though the aperture of the network is too narrow to permit strong conclusions. In contrast, shear strain rates and velocities in the Point Reyes-Petaluma arc show pronounced asymmetry, particularly between 1929 and 1939. As a consequence, we consider geologically reasonable models of deformation within the Point Reyes-Petaluma arc in more detail. We will compare these models to the available shear strain rate estimates (Figure 9) as these are our most fundamental results. Recall that estimated velocities are model coordinate velocities and therefore depend on a prior model. The velocity estimates at each station are also highly correlated with one another. This means that visual evaluations of inconsistencies between the prior model and the data can be deceiving because the eye cannot account for the existing correlations.

The first model, a purely secular model [*Bürgmann et al.*, 1994, 1997], provides a reference for subsequent models which incorporate additional sources of postseismic deformation. The purely secular model is clearly inconsistent with the shear strain rates during the earliest time interval, 1929-1939. Observed fault parallel shear strain rates (γ_1) are underpredicted within an ~20-km-wide zone extending to the northeast of the San Andreas fault (Figure 9a). Fault parallel shear strain rates to the northeast of the Rogers Creek fault are overpredicted. A purely secular model is more appropriate during the 1938-1961 time interval, though fault parallel shear strain rates near the San Andreas fault are still underpredicted (Figure 9b). The second model is the best fitting model with afterslip between 10 and 35 km depth (slip rates as in Figure 6). During the 1929-1939 time interval this model does a much better job of fitting the peak fault parallel shear strain rates at the San Andreas fault, but still does not satisfactorily describe the breadth of the postseismic deformation field to the northeast. Between 1938 and 1961 the deep afterslip model is very similar to the purely secular model, though in this case fault parallel shear strain rates near the San Andreas fault are slightly overpredicted. The third model, the best fitting 15-km-deep horizontal detachment surface, satisfactorily describes both the magnitude and spatial variation in the fault parallel shear strain between 1929 and 1939. During the 1938-1961 time interval the detachment model significantly overestimates fault-parallel strain rates between the San Andreas and Rogers Creek faults. Furthermore, while the presence of a horizontal detachment surface is predicted by some models of the thermomechanical evolution of the San Andreas fault system [*Furlong et al.*, 1989], it seems to contradict recent seismic reflection work in the San Francisco bay [*Parsons and Hart*, 1998] and northern California [*Henstock et al.*, 1997], which find evidence for discrete faults extending through the lower crust. None of the models fit the estimated γ_2 values very well (Figure 9). Thus these models do not seem completely satisfactory. In all cases, they fail to represent some portion of the data, and all have difficulty reproducing the time dependence of the deformation.

Other hypotheses have been put forth as an explanation for the asymmetry in the deformation field across the San Andreas fault. One involves differences in mechanical properties between oceanic and continental crust. *Lisowski et al.* [1991] investigated the effect of variations in material properties across the San Andreas fault in northern California using 1973-1989 trilateration data. They concluded that the required rigidity contrasts were unrealistic. Because the

asymmetry is enhanced immediately following the 1906 event, this problem would be exaggerated when attempting to describe the 1929-1939 data. A second option is the presence of a low-rigidity San Andreas fault zone. *Lisowski et al.* [1991] showed that existence of such a zone can effectively decouple the two sides of the fault, regardless of the contrast in material properties across it, though required rigidities within the fault zone may be too low to be realistic. Thus variations in material properties alone seem incapable of explaining the observed asymmetry.

Another possible explanation for the asymmetry is the occurrence of accelerated deep afterslip not only below the San Andreas fault but also below neighboring subparallel faults to the northeast. This would help explain the nearly constant fault parallel shear strain rates (i.e., the linear trend in fault-parallel velocity) to the northeast of the San Andreas fault. This linear trend, whose slope decreases with time, is apparent in each of the time intervals under consideration (Figure 8a). The modern velocity field can be effectively explained using a multiple fault dislocation model with deep slip beneath each of the three subparallel faults in northern California [*Freymueller et al.*, 1999; *Lisowski et al.*, 1991; *Prescott and Yu*, 1986]. It seems reasonable therefore to assume that the postseismic velocity fields could be explained in a similar fashion. The problem, as mentioned previously, is that the 1906 event moved neighboring subparallel faults away from failure. One would therefore not expect them to slip at faster rates. Fault-parallel shear strain rates in the subnetwork spanning the Rogers Creek fault are indeed lower between 1929 and 1939 as compared to the 1938-1961 time interval (Figure 5). On the other hand, if structures with low effective viscosities exist in the lower crust northeast of the San Andreas fault, they will increase the magnitude and spatial extent of time-dependent deformation in that direction [*Kenner and Segall*, 1999a]. The postseismic redistribution of stress will be governed by the spatial distribution of these low viscosity structures. As earthquake-induced stress gradients in the seismogenic crust are reduced, surface velocities to the northeast of the San Andreas fault will be increased [*Kenner and Segall*, 1999a]. This results in a deformation field that is asymmetric with respect to the San Andreas fault. Finally, if the San Andreas and Hayward-Rogers Creek-Maacama faults dip toward one another, as proposed by *Parsons and Hart* [1998], this will produce asymmetries that could also help to explain the observed distribution of deformation though time. Preliminary modeling indicates that faults with this geometry will concentrate postseismic deformation between them. At certain locations this can increase fault parallel strain accumulation rates [*Kenner and Segall*, 1999b]. In all probability, some combination of these mechanisms will be required to explain the asymmetry in the data through time.

Although our velocity estimates depend on a prior model to constrain rigid body translations, rotation, and scale, when they are combined with estimates of shear strain rate, we have better spatial resolution than previous results. In addition, these represent the only currently available velocity estimates for post-1906 deformation. Further, while the inversions do not provide well-constrained bounds on the depth distribution of slip (Plate 1), they do show how slip velocity varies with time (Figure 6). At both Point Arena and the Point Reyes-Petaluma arc, deformation rates decrease through time following the 1906 earthquake. This means that additional sources of deformation, beyond the simple secular model, are required to explain data from early in the earthquake cycle and that strain accumulation rates are temporally variable. In other words, geodetic measurements made many decades after a great event are not representative of the much higher loading rates immediately following a great earthquake.

5. Conclusions

In summary, we have used the methods of *Yu and Segall* [1996] to reanalyze historical triangulation data following the 1906 San Francisco earthquake. As this event provides one of the only sources of information regarding deformation following great earthquakes within the San Andreas fault system, any additional information, even if the uncertainties are large compared to more modern geodetic measurements, is extremely valuable in constraining existing models of postseismic deformation and lower crustal structure and rheology. This analysis has greatly increased both the temporal and spatial resolution of the applicable data in northern California.

The approach is most useful in the analysis of networks with short baselines such as the Point Arena and Point Reyes-Petaluma networks. Because the uncertainties grow with baseline length, networks with long baselines, such as the northern California primary network, did not generate reasonable velocity estimates. Unfortunately, this meant that efforts to obtain a postseismic velocity estimate for the Farallon Islands, 40 km to the southwest of the San Andreas fault, have been inconclusive.

With the addition of more recent geodetic results, we have been able to infer an effective exponential relaxation time for long-term postseismic deformation following the 1906 earthquake of 36 ± 16 years. This result agrees with the 30-year estimate of *Thatcher* [1983] using uniform shear strain rate data from the entire San Andreas fault system. Additionally, and for the first time, we have been able to make estimates of the post-1906 station velocities. Therefore we now have velocity profiles corresponding to each of the strain rate data points used in the estimates of relaxation time at Point Arena and Point Reyes.

The availability of localized shear strain rate measurements and individual station velocity estimates allows us to consider local variations in the spatial distribution of postseismic deformation following the 1906 San Francisco earthquake. Inferences concerning the appropriate models required to fit these data are mixed. Because of a lack of spatial resolution, particularly at Point Arena, inversions for the best fitting models are not well constrained, though, when taken in total, they do permit some conclusions. At both Point Arena and the Point Reyes-Petaluma arc the rate of deformation, on whatever structures are controlling the deformation, must change with time. At Point Arena the data can be satisfactorily fit with accelerated afterslip at depth along the San Andreas fault plane. For a 10-km-deep, 25-km-wide afterslip zone the average slip rate between 1906 and 1930 is 11.2 cm/yr. Between 1929 and 1975 it is 4.6 cm/yr. Inversions of the Point Arena data indicate that the width of the afterslip zone is unconstrained. If the characteristic coseismic slip is assumed to be < 5.5 m, then the top of the zone of accelerated afterslip must be shallower than 20 km. Data from the Point Reyes-Petaluma arc clearly show

asymmetric deformation with respect to the trace of the San Andreas fault, especially between 1929 and 1939. A closer look at geologically reasonable geometries, with slip rates determined from the inversion results, reveals that accelerated deep afterslip models do not explain particularly well the breadth of the deformation field to the northeast of the San Andreas fault, especially between 1929 and 1939. Both accelerated deep afterslip and horizontal detachment models have trouble explaining spatial variations in the deformation field through time. In other words, no single fault geometry can satisfactorily explain both the 1929-1939 and 1938-1961 data. As a result, some more complex mechanism, or combination of mechanisms, is needed to describe the Point Reyes-Petaluma arc results.

Acknowledgments. We thank Richard Snay for compiling the original dataset obtained from NGS, Mark Murray for his advice and help in analyzing the GPS data, and Roland Bürgmann for the use of his secular deformation model. Reviews by Wayne Thatcher, Roland Bürgmann, Stephanie Prejean, the Associate Editor, and an anonymous reviewer improved the manuscript. This work was supported by USGS grant 1434-HQ-97-GR-03122 and NSF grant EAR-9526910 to Stanford University.

References

Árnadóttir, T., and P. Segall, The 1989 Loma Prieta earthquake imaged from inversion of geodetic data, *J. Geophys. Res.*, *99*, 21,835-21,855, 1994.

Bomford, G., *Geodesy*, 4th ed., 855 pp., Clarendon, Oxford, 1980.

Bosl, W. J., Computational Studies of Crustal Fluids and Earthquakes, Ph.D. thesis, Stanford Univ., Stanford, Calif., 1999.

Bürgmann, R., R. Arrowsmith, T. Dumitru, and R. McLaughlin, Rise and fall of the southern Santa Cruz Mountains, California, deduced from fission track dating, geomorphic analysis, and geodetic data, *J. Geophys. Res.*, *99*, 20,181-20,202, 1994.

Bürgmann, R., P. Segall, M. Lisowski, and J. Svarc, Postseismic strain following the 1989 Loma Prieta earthquake from GPS and leveling measurements, *J. Geophys. Res.*, *102*, 4933-4955, 1997.

Cline, M. W., R. A. Snay, and E. L. Timmerman, Geodetically derived strain from San Francisco bay to the Mendocino triple junction, California, *NOAA Tech. Rep. NOS 109 NGS 31*, 17 pp., Natl. Oceanic and Atmos. Admin., Silver Springs, Md., 1985.

Deng, J., M. Gurnis, H. Kanamori, and E. Hauksson, Viscoelastic flow in the lower crust after the 1992 Landers, California, earthquake, *Science*, *282*, 1689-1692, 1998.

Donnellan, A., and G. A. Lyzenga, GPS observations of fault afterslip and upper crustal deformation following the Northridge earthquake, *J. Geophys. Res.*, *103*, 21,285-21,297, 1998.

Freymueller, J. T., M. H. Murray, P. Segall, and D. Castillo, Kinematics of the Pacific-North American plate boundary zone, northern California, *J. Geophys. Res.*, *104*, 7419-7441, 1999.

Furlong, K. P., W. D. Hugo, and G. Zandt, Geometry and evolution of the San Andreas fault zone in northern California, *J. Geophys. Res.*, *94*, 3100-3110, 1989.

Gilbert, L. E., J. Beavan, and C. H. Scholz, Analysis of a 100 year geodetic record from northern California, in *Contributions of Space Geodesy to Geodynamics: Crustal Dynamics, Geodyn. Ser.*, vol. 23, edited by D. E. Smith and D. L. Turcotte, pp. 215-232, AGU, Washington, D. C., 1993.

Henstock, T. J., A. Levander, and J. A. Hole, Deformation in the lower crust of the San Andreas fault system in northern California, *Science*, *278*, 650-653, 1997.

Holbrook, W. S., T. M. Brocher, U. S. ten Brink, and J. A. Hole, Crustal structure of a transform plate boundary: San Francisco and the central California continental margin, *J. Geophys. Res.*, *101*, 22,311-22,334, 1996.

Jaumé, S. C., and L. R. Sykes, Evolution of moderate seismicity in the San Francisco Bay region, 1850 to 1993: Seismicity changes related to the occurrence of large and great earthquakes, *J. Geophys. Res.*, *101*, 765-789, 1996.

Kelson, K. I., W. R. Lettis, and M. Lisowski, Distribution of geologic slip and creep along faults in the San Francisco bay region, in *Proceedings of the Second Conference on Earthquake Hazards in the Eastern San Francisco Bay Area*, edited by G. Borchardt et al., *Spec. Publ. 113*, pp. 31-38, Calif. Dep. of Conserv., Div. of Mines and Geol., Sacramento, 1992.

Kenner, S. J., and P. Segall, Time-dependence of the stress shadowing effect and its relation to the structure of the lower crust, *Geology*, *27*, 119-122, 1999a.

Kenner, S. J., and P. Segall, Time varying velocities following the 1906 San Francisco earthquake: the role of postseismic relaxation processes in the lower crust (abstract), *Eos Trans. AGU*, *80* (17), Spring Meet. Suppl., S325-S326, 1999b.

Li, V. C., and J. R. Rice, Crustal deformation in great California earthquake cycles, *J. Geophys. Res.*, *92*, 11,533-11,551, 1987.

Lisowski, M., and J. C. Savage, The velocity field in the San Francisco bay area and the inferred depth of creep on the Hayward fault, in *Proceedings of the Second Conference on Earthquake Hazards in the Eastern San Francisco Bay Area*, edited by G. Borchardt et al., *Spec. Publ. 113*, pp. 39-44, Calif. Dep. of Conserv., Div. of Mines and Geol., Sacramento, 1992.

Lisowski, M., J. C. Savage, and W. H. Prescott, The velocity field along the San Andreas fault in central and southern California, *J. Geophys. Res.*, *96*, 8369-8389, 1991.

Matthews, M. V., and P. Segall, Estimation of depth-dependent fault slip from measures surface deformation with application to the 1906 San Francisco earthquake, *J. Geophys. Res.*, *98*, 12,153-12,163, 1993.

Menke, W., *Geophysical Data Analysis: Discrete Inverse Theory, Int. Geophys. Ser.*, vol. 45, rev. ed., 285 pp., Academic, San Diego, Calif., 1989.

Murray, M. H., W. H. Prescott, R. Bürgmann, J. T. Freymueller, P. Segall, J. Svarc, S. D. P. Williams, M. Lisowski, and B. Romanowicz, The deformation field of the Pacific-North American plate boundary zone in northern California from geodetic data, 1972-1998 (abstract), *Eos Trans. AGU*, *79* (45), Fall Meet. Suppl., F192, 1998.

Nur, A., and G. Mavko, Postseismic viscoelastic rebound, *Science*, *183*, 204-206, 1974.

Parsons, T., and P. E. Hart, Dipping San Andreas and Hayward faults revealed beneath San Francisco Bay, California, *Geology*, 27, 839-842, 1999.

Peltzer, G., P. Rosen, F. Rogez, and K. Hudnut, Postseismic rebound in fault step-overs caused by pore fluid flow, *Science*, *273*, 1202-1204, 1996.

Peltzer, G., P. Rosen, and F. Rogez, Poroelastic rebound along the Landers 1992 earthquake surface rupture, *J. Geophys. Res.*, *103*, 30,131-30,145, 1998.

Pollitz, F. F., and I. S. Sacks, Modeling of postseismic relaxation following the great 1857 earthquake, southern California, *Bull. Seismol. Soc. Am.*, *82*, 454-480, 1992.

Pollitz, F. F., R. Bürgmann, and P. Segall, Joint estimation of afterslip rate and postseismic relaxation following the 1989 Loma Prieta earthquake, *J. Geophys. Res.*, *103*, 26,975-26,992, 1998.

Pollitz, F. F., G. Peltzer, and R. Bürgmann, Mobility of continental mantle: Evidence from postseismic geodetic observations following the 1992 Landers earthquake, *J. Geophys. Res.*, *105*, 8035-8054, 2000.

Prescott, W. H., and S. Yu, Geodetic measurement of horizontal deformation in the northern San Francisco bay region, California, *J. Geophys. Res.*, *91*, 7475-7484, 1986.

Savage, J. C., Equivalent strike-slip earthquake cycles in half-space and lithosphere-asthenosphere Earth models, *J. Geophys. Res.*, *95*, 4873-4879, 1990.

Savage, J. C., and W. H. Prescott, Asthenospheric readjustment and the earthquake cycle, *J. Geophys. Res.*, *83*, 3369-3376, 1978.

Savage, J. C., and J. L. Svarc, Postseismic deformation associated with the 1992 M_w = 7.3 Landers earthquake, southern California, *J. Geophys. Res.*, *102*, 7565-7577, 1997.

Savage, J. C., M. Lisowski, and J. L. Svarc, Postseismic deformation following the 1989 (M = 7.1) Loma Prieta, California, earthquake, *J. Geophys. Res.*, *99*, 13,757-13,765, 1994.

Savage, J. C., J. L. Svarc, and W. H. Prescott, Geodetic estimates of fault slip rates in the San Francisco Bay area, *J. Geophys. Res.*, *104*, 4995-5002, 1999.

Segall, P., and M. V. Matthews, Displacement calculations from geodetic data and the testing of geophysical deformation models, *J. Geophys. Res.*, *93*, 14,954-14,966, 1988.

Shen, Z.-K., D. D. Jackson, Y. Feng, M. Cline, M. Kim, P. Fang, and Y. Bock, Postseismic deformation following the Landers earthquake, California, 28 June 1992, *Bull. Seismol. Soc. Am.*, *84*, 780-791, 1994.

Simpson, R. W., and P. A. Reasenberg, Earthquake-induced static stress changes on central California faults, in *The Loma Prieta, California, earthquake October 17, 1989: Tectonic Processes and Models*, edited by R. W. Simpson, *U.S. Geol. Surv. Prof. Pap., 1550F*, F55-F89, 1994.

Thatcher, W., Strain accumulation and release mechanism of the 1906 San Francisco earthquake, *J. Geophys. Res.*, *80*, 4862-4872, 1975a.

Thatcher, W., Strain accumulation on the northern San Andreas fault zone since 1906, *J. Geophys. Res.*, *80*, 4873-4880, 1975b.

Thatcher, W., Nonlinear strain buildup and the earthquake cycle on the San Andreas fault, *J. Geophys. Res.*, *88*, 5893-5902, 1983.

Thatcher, W., G. Marshall, and M. Lisowski, Resolution of fault slip along the 470-km-long rupture of the great 1906 San Francisco earthquake and its implications, *J. Geophys. Res.*, *102*, 5353-5367, 1997.

Williams, S. D. P., Current motion on faults of the San Andreas system in central California inferred from recent GPS and terrestrial survey measurements, Ph.D. thesis, Univ. of Durham, Durham, England, 1995.

Williams, S. D. P., J. L. Svarc, M. Lisowski, and W. H. Prescott, GPS measured rates of deformation in the northern San Francisco bay region, California, 1990-1993, *Geophys. Res. Lett.*, *21*, 1511-1514, 1994.

Wyatt, F. K., D. C. Agnew, and M. Gladwin, Continuous measurements of crustal deformation for the 1992 Landers earthquake sequence, *Bull. Seismol. Soc. Am.*, *84*, 768-779, 1994.

Yu, E., and P. Segall, Slip in the 1868 Hayward earthquake from the analysis of historical triangulation data, *J. Geophys. Res.*, *101*, 16,101-16,118, 1996.

S. J. Kenner and P. Segall, Department of Geophysics, Stanford University, Mitchell Building, Stanford, CA 94305-2215 (kenner@geo.stanford.edu; segall@geo.stanford.edu)

(Received June 28, 1999; revised January 31, 2000; accepted March 2, 2000)